JITUO LIU[1], XIANHUI WANG[1]*, JIA LIU[1], QIANNI RAN[1]

THE EFFECT OF HEAT TREATMENT ON THE MICROSTRUCTURE EVOLUTION AND PROPERTIES OF AN AGE-HARDENED Cu-3Ti-2Mg ALLOY

The study investigates the effect of heat treatment on the microstructure evolution and properties of an age-hardened Cu-3Ti-2Mg alloy. The precipitated Cu_2Mg and β'-Cu_4Ti phases consequently yield a depletion of the Cu matrix in regards to Ti and Mg solutes, which enhances the electrical conductivity. The Cu_2Mg Laves phase and β'-Cu_4Ti phase precipitates increase the hardness of the alloy due to the consistency and coherency of the later phase. However, the decrease of hardness is mainly associated with the coarse microstructures, that can be formed due to the phase transformation from metastable β'-Cu_4Ti phase to more stable Cu_3Ti phase. In the range of experiments, the optimum process is solution treatment at 700°C for 4 h, with subsequent age-hardening at 450°C for 4 h. The electrical conductivity, hardness, tensile strength, and elongation of the Cu-3Ti-2Mg alloy were 15.34 %IACS, 344 HV, 533 MPa, and 12%, respectively.

Keywords: Cu alloy, aging treatment, microstructure, precipitation, electrical conductivity

1. Introduction

The extensive application of copper alloys originates from its favorable electrical and thermal conductivity, strength, elastic modulus, and excellent integrated performance [1-4]. The Cu-Be, among other copper alloys, offers an excellent combination of electrical and mechanical responses. However, its toxicity brings about environmental concerns fostering the development of new environmentally, friendly substitutional materials [5,6]. Hence, the alloys based on Cu-Ti as age-hardening material are promising for replacement of Cu-Be alloys.

The age-hardenable Cu-Ti alloy with 1-5 wt.% Ti exhibits adequate mechanical properties to substitute expensive and toxic Cu-Be alloy [7]. The relation between phase composition and mechanical properties of Cu-Ti alloys is under extensive research. The spinodal decomposition has been shown to be an underpinning mechanism behind precipitation strengthening of Cu-Ti alloys upon aging [8]. The precipitation mechanism in Cu-Ti alloy shows that at proper aging conditions, the strengthening is favored by the formation of a metastable β'-Cu_4Ti phase. The phase transformation of metastable, coherent β'-Cu_4Ti into an equilibrium, incoherent Cu_3Ti phase will occur during over-aging, which substantially decreases the strength of Cu-Ti

alloy. In addition, the electrical conductivity of the Cu-Ti alloy decreases due to a high concentration of Ti solutes in the Cu-matrix [9]. Therefore, it is critical for electronic engineering to improve the electrical conductivity of Cu-Ti alloys. At proper aging conditions, Wang et al. reported enhanced the electrical conductivity of the Cu-3Ti-2Sn of 23.1 Ms/m, which is 5.25 times higher than that of an as-cast alloy [10,11]. The hardness also increases from 98.6 to 134.5 HV, but it is still not satisfying. Markandeya et al. reported that the Cu-4Ti-1Cr alloy acquires hardness of 326 HV on peak aging, whereas the electrical conductivity is only 8.8 %IACS [12]. Markandeya et al. also revealed that the Cd addition improves the mechanical properties of the Cu-3Ti alloy but impairs its electrical conductivity [13]. All these studies clearly show that age-hardening of Cu-Ti alloys yields a continuous, coherent, and metastable β'-Cu_4Ti precipitate at the proper aging conditions, but still, simultaneous achievement of high electrical conductivity and hardness is not a straightforward procedure.

Mg is an abundant element and has a small relative atomic mass [14]. Meanwhile, Maki et al. found that the Mg supersaturation can provide high electrical conductivity and strength of the Cu matrix [15]. The solution-drag effect of Mg atoms on dislocation motion was previously suggested as a plausible

---

[1]   XI'AN UNIVERSITY OF TECHNOLOGY, SCHOOL OF MATERIALS SCIENCE AND ENGINEERING, SHAANXI PROVINCE KEY LABORATORY OF ELECTRICAL MATERIALS AND INFILTRATION TECHNOLOGY, XI'AN 710048, P.R. CHINA

*   Corresponding author: xhwang693@xaut.edu.cn

164

strengthening mechanism [16,17]. Therefore, the design of the Cu-3Ti-2Mg alloy aims to provide high electrical conductivity and hardness in the same material. The precipitation behavior of the Cu-3Ti-2Mg alloy was analyzed in this study, accompanied by a detailed microstructural and phase composition characterization, in order to develop an alloy with an appropriate balance of mechanical and electrical conductivity properties.

2. Experimental procedures

Purity 99.9 wt.% Cu, purity 99.9 wt.% Ti, and the purity 99.9 wt.% Cu15Mg master alloy were used as starting materials. A Cu-3 wt.% Ti-2 wt.% Mg ingot was prepared in a graphite crucible using an intermediate frequency induction furnace under the Ar protecting environment. The ingot was sliced into blocks which were then exposed to a solution treatment at 650, 700, 750, and 800°C for 4 h in an SK-2.5-13S tube furnace, with subsequent quenching in water. Afterward, the samples were aged at 350, 400, 450, 500, and 550°C for 4 h, and then aged at 450°C for 1, 2, 4, 6, and 8 h in Ar atmosphere. As-prepared samples were ground with abrasive papers of different grits. Mechanically polished samples were etched electrochemically for 5-10 s at 2 V and 0.4 A in a 30 wt.% phosphoric acid solution. Morphological and phase analyses were performed by optical microscopy (OM), a scanning electron microscopy (SEM, JSM-6700F, and Zeiss-Merlin) and transmission electron microscopy (TEM, JEM-3010) techniques. The preparation of samples for TEM included a low-speed cutting and mechanical polishing down to 50 μm thick slices, which were punched to obtain discs with 3 mm in diameter. Finally, an M691 ion milling at 4.5 kV, with an incident angle of 6° was used for thinning the samples. The electrical conductivity was tested by FQR-7501 eddy conductivity gauge and hardness was determined at a load of 10 kg holding for 10 s on an HV-1000 hardness testing machine. Tensile tests were performed using a universal test machine (HT-2402) at a strain rate of 1 mm/min.

3. Results and discussion

Fig. 1 shows the starting microstructures of Cu-3Ti alloy and Cu-3Ti-2Mg alloy ingots. It can be seen that the microstructure consists of dendrite grains, which appears a gray skeleton, while the space between the dendrite skeleton appears as black. The Mg addition increased the primary phase between the dendrite skeleton (Fig. 1(a) and Fig. 1(b)). The hardness and electrical conductivity of the Cu-3Ti alloy ingot are 130 HV and 9.2 %IACS, respectively. However, 2% Mg addition enhances the hardness and electrical conductivity, which are respectively increased to 279 HV and 12.5 %IACS. In addition, the dendrite grains are harmful to subsequent aging treatment. To remove the dendrite structures and obtain a supersaturated solid solution, a solution treatment at different temperatures for 4 h was conducted. Fig. 2 shows the microstructures of as-cast Cu-3Ti-2Mg alloy treated at 650, 700, 750, and 800°C for 4 h. From Fig. 2, the dendrite structures were eliminated after solution treatment at 700°C for 4 h (Fig. 2(b)), being re-dissolved into the Cu matrix. However, the dendrite structures appeared at the grain boundary if the as-cast Cu-3Ti-2Mg alloy is solution treated at 750 and 800°C (Fig. 2(c) and Fig. 2(d)). This originates from the re-dissolution of the grain boundary Mg into the Cu matrix at high temperature and the dendritic structure forms during the water quenching process, which indicating that the alloy composition is uneven. Therefore, for the formation of a supersaturated solid solution, the most appropriate temperature was 700°C in the investigated temperature range from 650 to 800°C. Figs. 3(a)-(b) are SEM micrographs of the as-cast Cu-3Ti-2Mg alloy solution treated at 700°C for 4 h. It can be seen from Fig. 3(b) that the grain boundary has a lamellar structure.

Figs. 4(a)-(c) shows SEM micrographs of the Cu-3Ti-2Mg alloy aged at 350, 450, and 550°C for 4 h. The grain sizes do not change with the increase of aging temperature, while the number of irregular particles at grain boundary increases. Interestingly, a few irregular particles and the lamellar structure appeared at the grain boundary after aging at 350°C for 4 h, Fig. 4(a1). By the further increase of aging temperature, the lamellar structure disappears compared to the solid solution (Fig. 4(b1)). The ir-
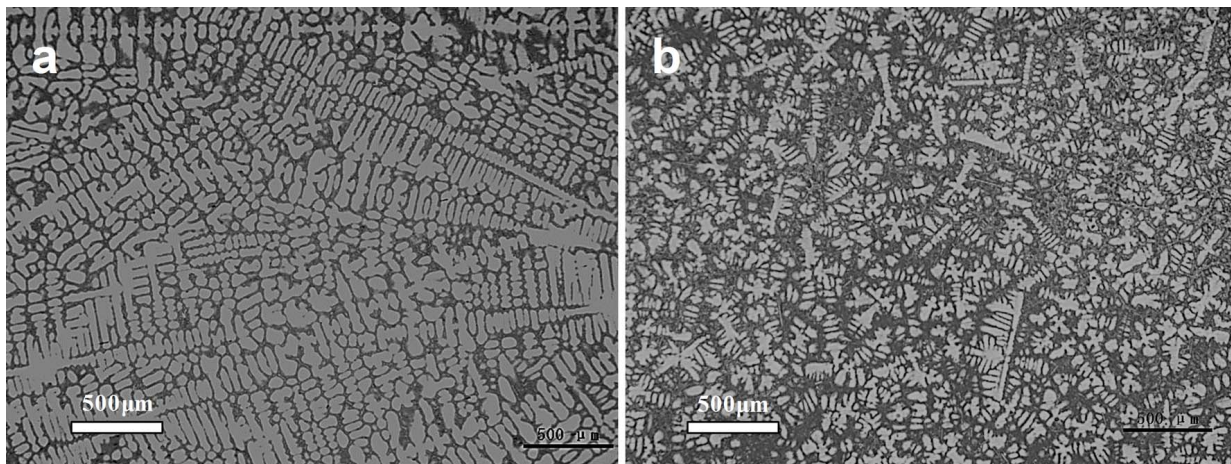

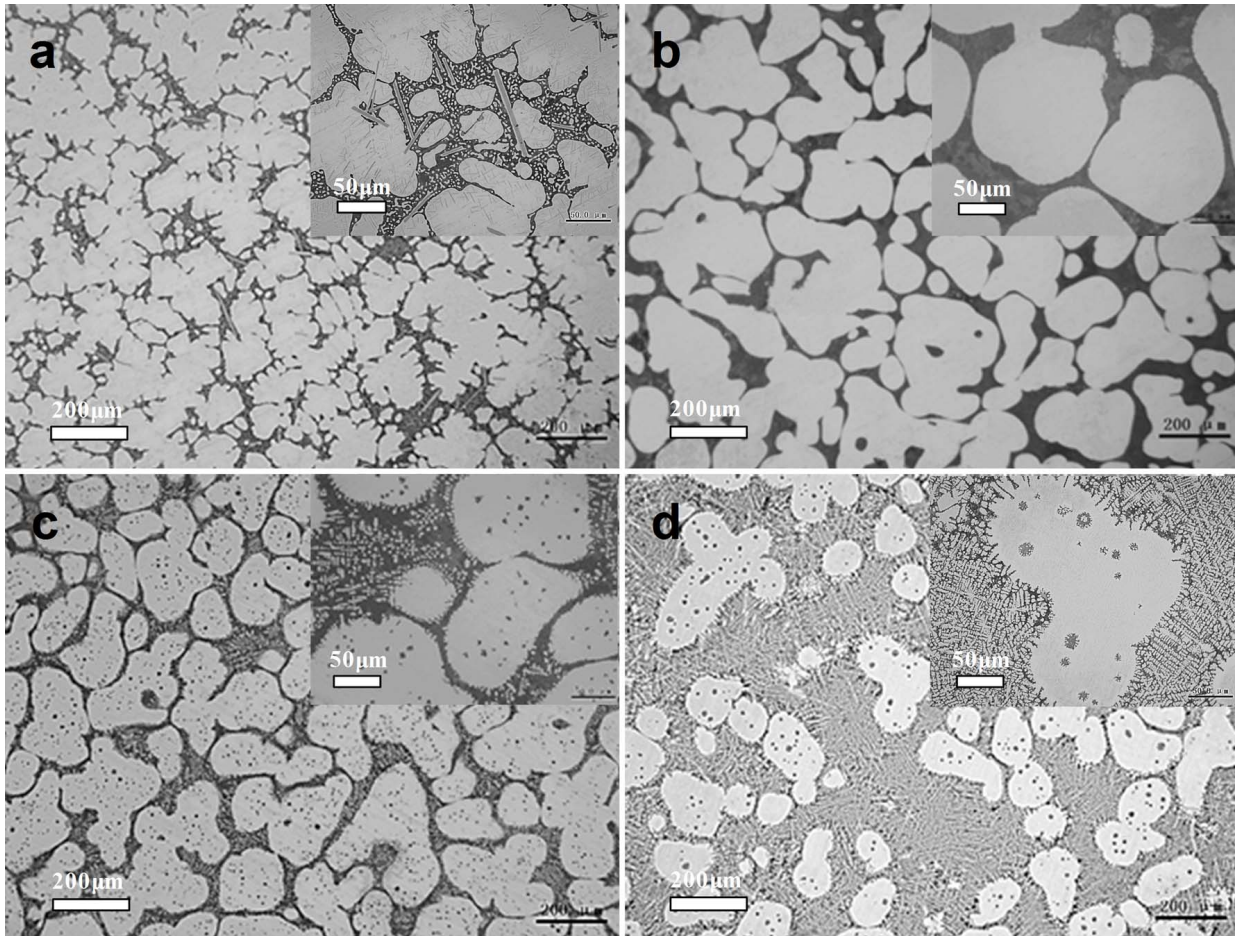Fig. 1. As-cast microstructures of Cu-3Ti (a) and Cu-3Ti-2Mg alloys (b)

Fig. 2. Microstructures of as-cast Cu-3Ti-2Mg alloy after the solution treatment at different temperatures for 4 h: (a) 650°C; (b) 700°C; (c) 750°C; (d) 800°C
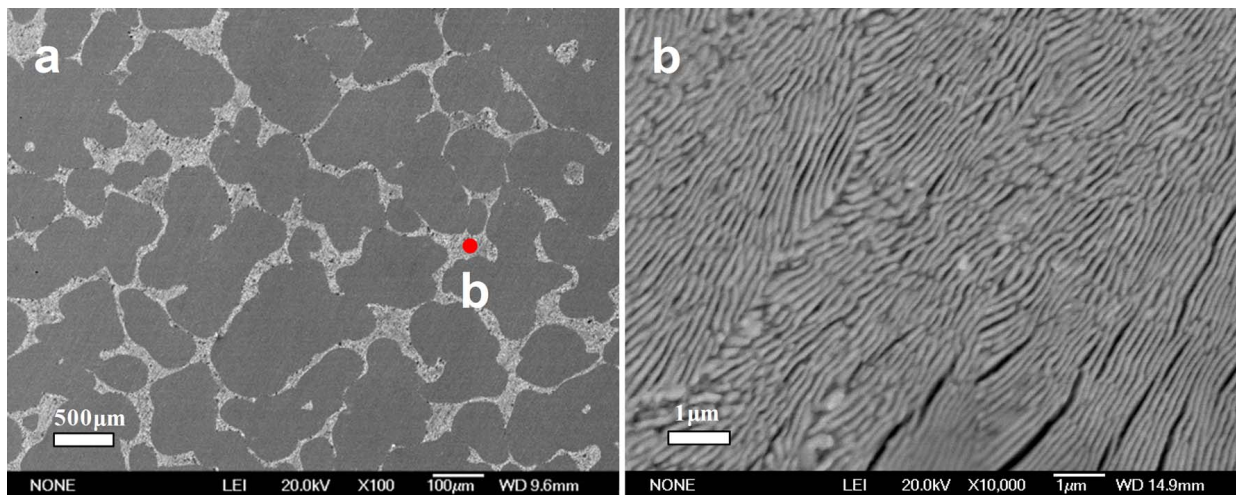

Fig. 3. SEM micrographs of the as-cast Cu-3Ti-2Mg alloy after the solution treatment at 700 °C for 4 h: (a) low magnification; (b) high magnification marked in Fig. 3(a)

regular particles are coarsened apparently after aging at 550°C for 4 h (Fig. 4(c1)). Therefore, 450°C was the most appropriate aging treatment temperature in the investigated temperature range from 350 to 550°C. This is because that the amount of precipitated phase is less at lower aging temperature, and the precipitates are easy to coarsen at higher aging temperature.

The TEM analysis of two specimens after aging at 450°C (Fig. 5) and 550°C (Fig. 6) for 4 h, reveals the composition, size, and morphology of the precipitates of the aged Cu-3Ti-2Mg alloy. Figs. 5(a)-(b) are the TEM micrograph and the corresponding SAED pattern of the Cu-3Ti-2Mg alloy aged at 450°C for 4 h. An ellipsoidal precipitated phase with a length of about 500 nm
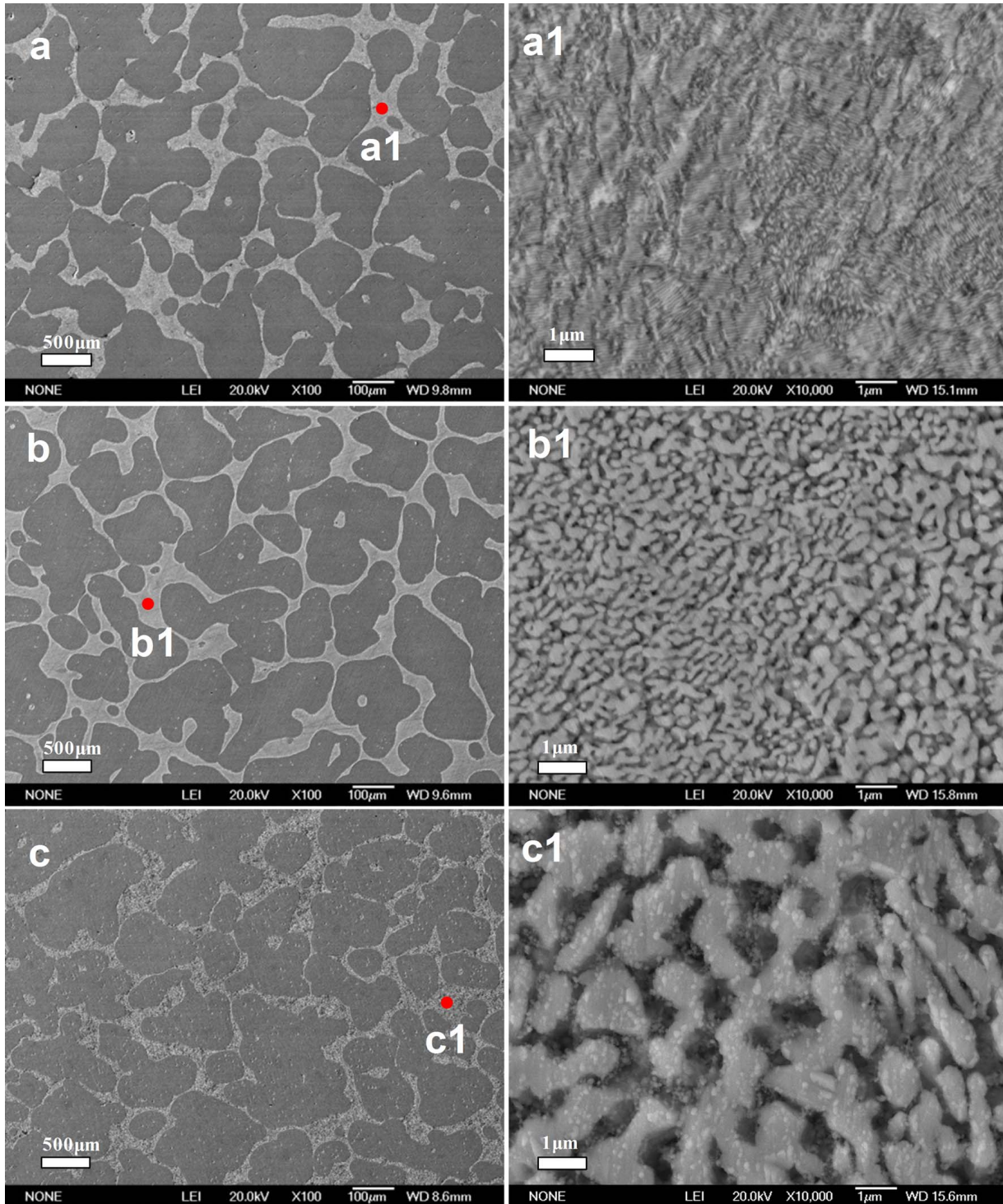
Fig. 4. SEM micrographs of the Cu-3Ti-2Mg alloy aged at different temperature for 4 h: (a)(a1) 350°C; (b)(b1) 450°C; (c)(c1) 550°C. (Fig. 4(a1), Fig. 4(b1) and Fig. 4(c1) are marked in Fig. 4(a), Fig. 4(b) and Fig. 4(c), respectively.)

appeared, accompanied by a number of tiny black particles. The ellipsoidal phase is Cu_2Mg, with a cubic crystal structure (lattice parameters: $a = 0.7047$ nm, $b = 0.7047$ nm, $c = 0.7047$ nm). The black particles are plausibly a continuous, coherent, and metastable β'-Cu_4Ti phase, with a body-centered tetragonal crystal structure (prototype: Ni_4Mo, space group: I4/m, lattice parameters: $a = 0.584$ nm, $b = 0.584$ nm, $c = 0.362$ nm), which corroborates well with the previously reported results by Markandeya and Semboshi et al [18-21].

Fig. 6(a) and Fig. 6(c) are the TEM micrographs of the Cu-3Ti-2Mg alloy aged at 550°C for 4 h. Fig. 6(b) and Fig. 6(d) are the corresponding SAED patterns, respectively. Obviously, the lamellar phase is present in the Cu matrix (Fig. 6(a)), which is determined (Fig. 6(b)) to be a discontinuous, incoherent, and stable Cu_3Ti phase with an orthorhombic crystal structure (lattice parameters: $a = 0.545$ nm, $b = 0.442$ nm, $c = 0.430$ nm), being is in accordance with the result reported by Markandeya [22-24]. It is believed that the coherent and metastable β'-Cu_4Ti
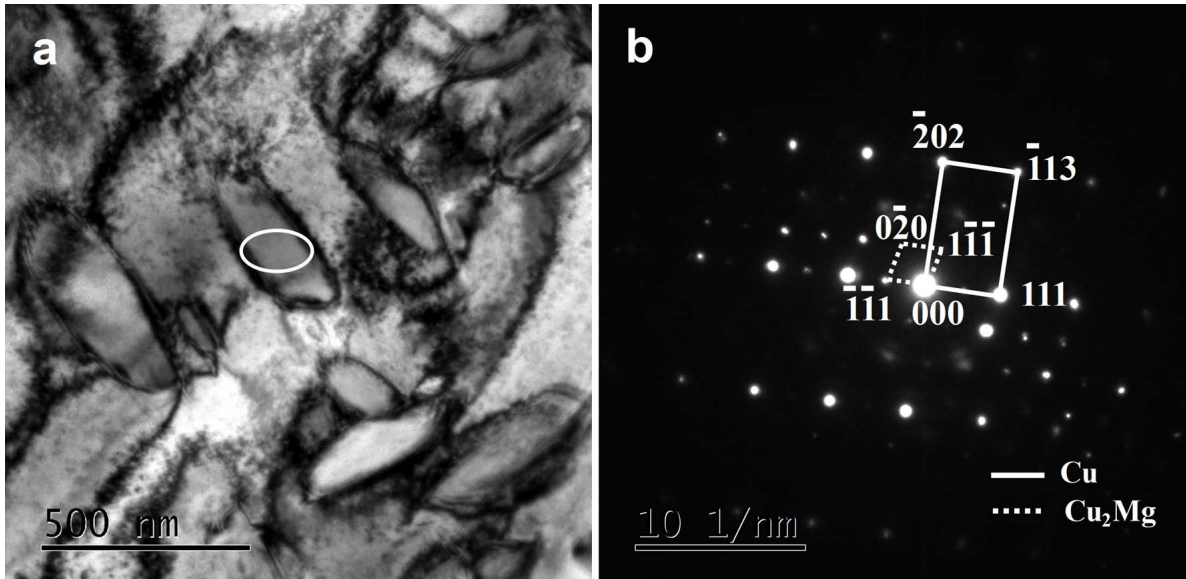
Fig. 5. The TEM micrograph (a) and the corresponding SAED pattern (b) of the Cu-3Ti-2Mg alloy aged at 450°C for 4 h
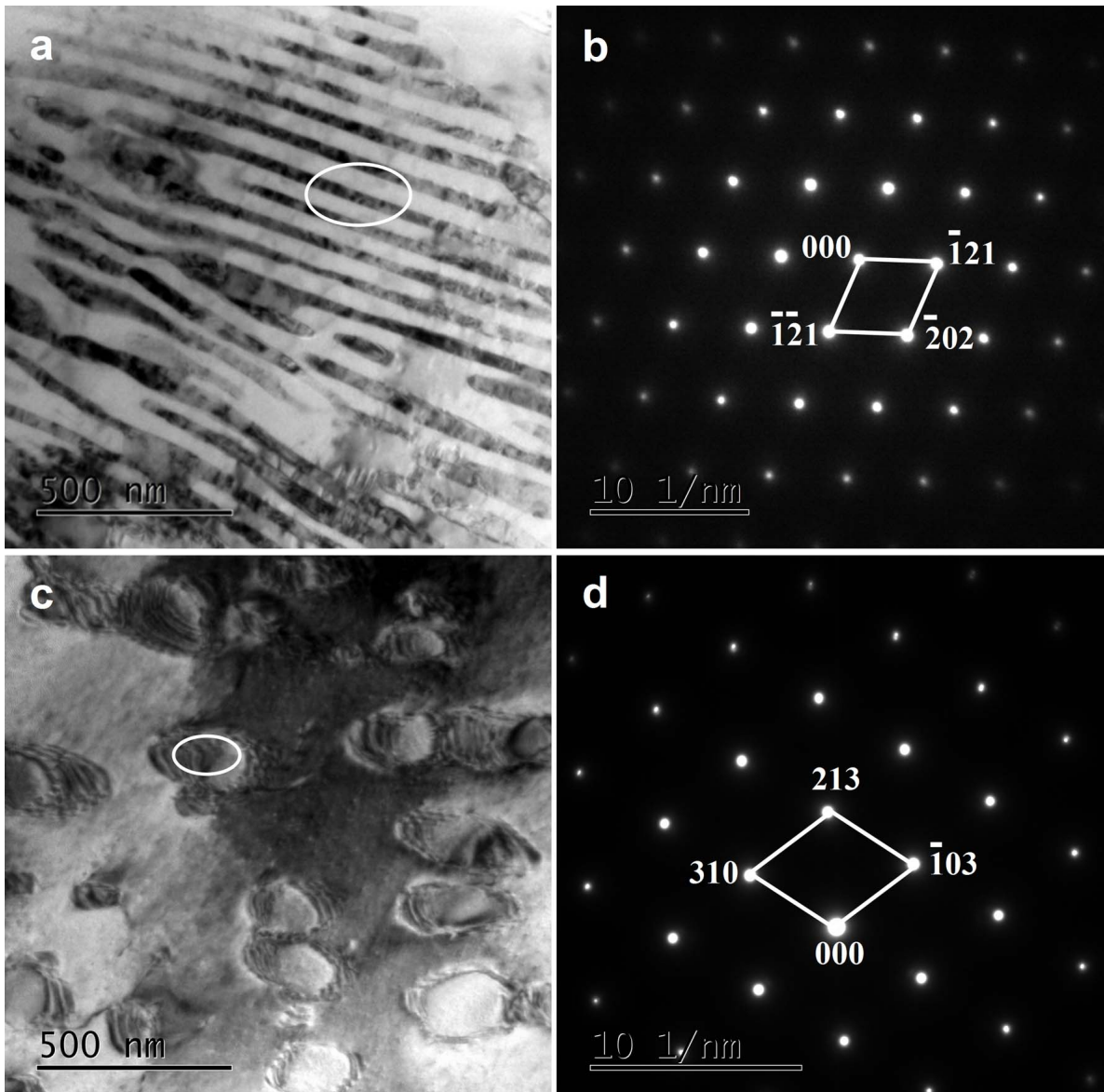

Fig. 6. TEM micrographs (a, c) and corresponding SAED patterns (b, d) of the Cu-3Ti-2Mg alloy aged at 550°C for 4 h

phase can contribute to the strengthening effect during aging, while too long aging time and high aging temperature cause the β'-Cu$_4$Ti phase to change into the equilibrium and incoherent Cu$_3$Ti phase, which essentially decreases the strength of the Cu-Ti alloy. Fig. 6(c) is a TEM micrograph of dislocation loops of the Cu-3Ti-2Mg alloy aged at 550°C for 4 h. As evident from Fig. 6(d), many dislocation loops are located around Cu$_2$Mg phase, which is probably caused by the vacancy formation at high aging temperature.

The influence of aging temperature on electrical conductivity and hardness of the Cu-3Ti-2Mg alloy is shown in Fig. 7(a). The electrical conductivity increases remarkably to 15.34 %IACS after aging at 450°C for 4 h. However, it decreases by 13.45% after aging at 550°C for 4 h. On the other side, the hardness reaches 344 HV after aging 450 °C for 4 h (shown Table 1). Fig. 7(b) shows the influence of aging time on electrical conductivity and hardness variations. At the early stage, both functional properties sharply increase with a subsequent slowly down of the trend. At 450°C for 4 h, the hardness decreases, while the electrical conductivity slightly increases with the aging time. After 8 h at 450°C, the electrical conductivity increases to 15.7 %IACS and the hardness decreases to 293 HV (shown Table 1).

The amount of solute atoms in the Cu matrix critically affects the electrical conductivity [25,26]. At the initial aging phase, the supersaturated Cu-3Ti-2Mg alloy has high precipita-

tion energy and accelerates the precipitation of Ti and Mg atoms that rapidly transform into Cu$_2$Mg and β'-Cu$_4$Ti secondary phases. This reduces the concentration of alloy atoms in the solid solution, relieves the lattice distortion of the Cu matrix, decreases electron scattering, and increases the electrical conductivity of the Cu-3Ti-2Mg alloy [27,28]. Thus, the Cu-3Ti-2Mg alloy has a better electrical performance with prolonged aging. However, the elevated temperature promotes the precipitated atoms to re-dissolve in the matrix, remarkably reducing the electrical conductivity.

During the aging of the Cu-3Ti-2Mg alloy, a large quantity of secondary Cu$_2$Mg and β'-Cu$_4$Ti phases precipitate. The topological structure of Cu$_2$Mg Laves phase poses high hardness and hinders the motion of dislocations, which has a large influence on the hardness. Moreover, the precipitated but structured β'-Cu$_4$Ti phase is coherent with the Cu matrix, which is the main factor of the hardness increase [29]. Hence, the hardness of Cu-3Ti-2Mg alloy progressively increases until its peak value is reached. Upon over-aging, both elevated temperature and time, the hardness critically decreases. It can be explained as follows. Firstly, the microstructure of grain boundary and the precipitated Cu$_2$Mg phase coarsen. Secondly, the coherent β'-Cu$_4$Ti phase transformed into the incoherent Cu$_3$Ti phase. Hence, the hardness of the Cu-3Ti-2Mg alloy sharply decreases under the function of various factors.
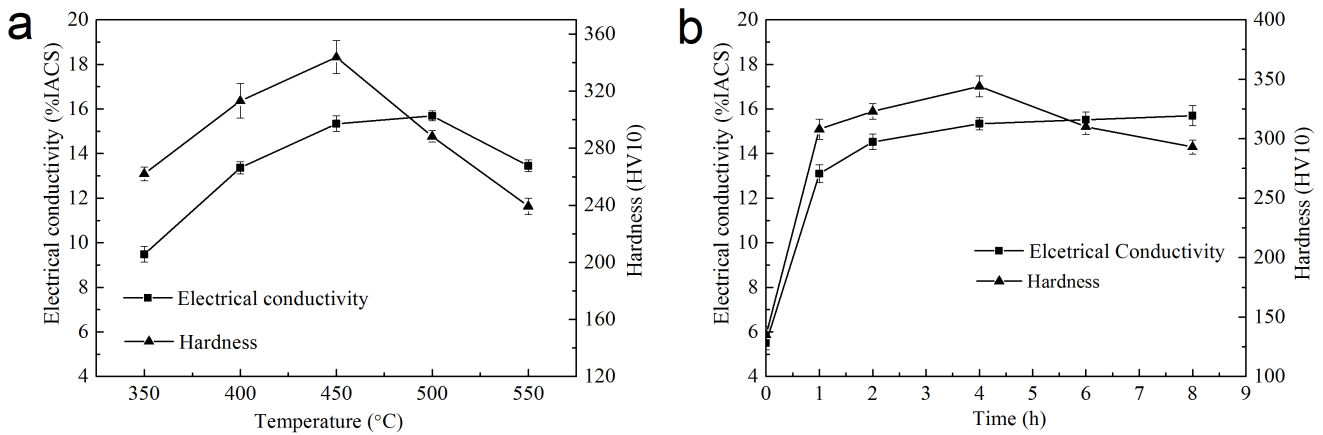

Fig. 7. The change of electrical conductivity and hardness of the Cu-3Ti-2Mg alloy with different aging temperature for 4 h (a) and aged at 450°C for different time (b)

TABLE 1

The properties of Cu-3Ti-2Mg alloy with different heat treatment processes

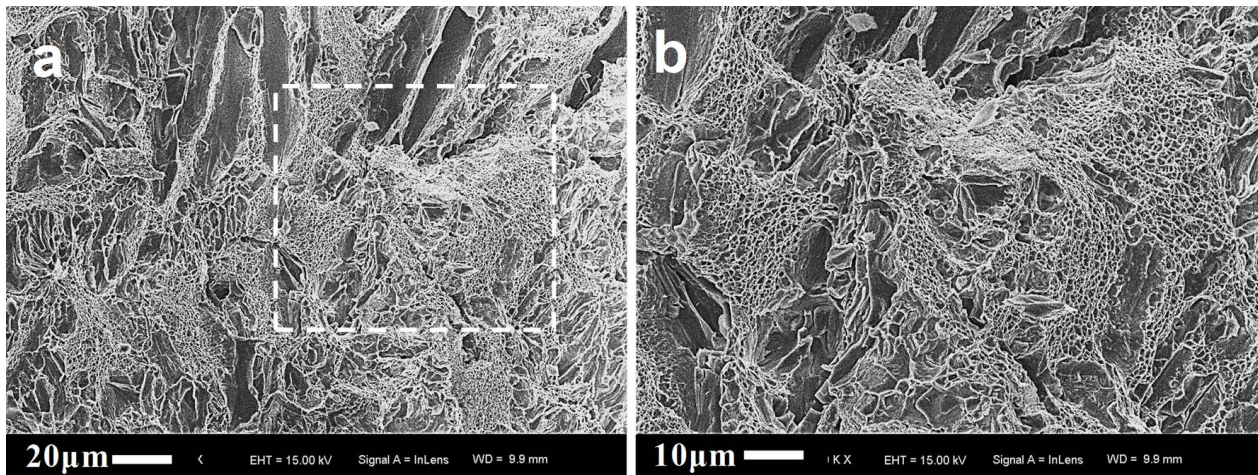| Heat treatment processes	Hardness (HV10)	Electrical conductivity (%IACS)	Tensile strength (MPa)	Elongation (%)
350°C / 4 h	262	9.48	456	23
400°C / 4 h	313	13.36	521	15
450°C / 4 h	344	15.34	533	12
500°C / 4 h	288	15.69	487	20
550°C / 4 h	239	13.45	432	23
450°C / 1 h	308	13.1	514	19
450°C / 2 h	323	14.52	524	14
450°C / 6 h	310	15.52	519	17
450°C / 8 h	293	15.7	491	19

Fig. 8. SEM fracture morphology at different magnifications for the Cu-3Ti-2Mg after aging at 450°C for 4 h

Tensile tests were performed to estimate the mechanical response, and the results are listed in Table 1. Obviously, the optimum process is solution treatment at 700°C for 4 h, with subsequent age-hardening at 450°C for 4 h in the range of experiments. The electrical conductivity, hardness, tensile strength, and elongation of the Cu-3Ti-2Mg alloy were 15.34 %IACS, 344 HV, 533 MPa, and 12%, respectively. The hardness, electrical conductivity and tensile strength of the Cu-3Ti-2Mg alloy are expected to be greater than 330 HV, 18 %IACS and 587 MPa in this experiment [10,15,16]. The hardness and electrical conductivity of Cu-3Ti-2Mg alloy are close to those of Maki et al [15] and Yang et al [16], but the tensile strength is low, which needs further research.

Fig. 8 shows the fracture morphology at different magnifications for the Cu-3Ti-2Mg alloy after aging at 450°C for 4 h. Apparently, a hybrid fracture mode of the Cu-3Ti-2Mg alloy was present, showing the morphology of a cleavage fracture simultaneously with a ductile fracture and the appearance of dimples. Hence, it is suggested that the failure mechanism of the alloy is a mixed one, including a quasi-cleavage fracture and a ductile fracture.

4. Conclusions

The precipitated Cu_2Mg and β'-Cu_4Ti phases are beneficial for the improvement of the electrical conductivity and hardness of the Cu-3Ti-2Mg alloy. Over-aging lead to the transformation of the continuous, coherent, and metastable β'-Cu_4Ti phase into discontinuous, incoherent, and stable Cu_3Ti phase, thus decreasing the hardness of the Cu-3Ti-2Mg alloy. In the investigated experimental range, the electrical conductivity, hardness, tensile strength, and elongation of the Cu-3Ti-2Mg alloy are 15.3 %IACS, 344 HV, 533 MPa, and 12%, respectively, after aging at 450°C for 4 h.

REFERENCES

[1] S. Li, Z. Li, Z. Xiao, S.H. Li, L.N. Shen, Q.Y. Dong, Mater. Sci. Eng. A **650** (5), 345-353 (2016).

[2] L. Gomidželović, E. Požega, A. Kostov, N. Vuković, V. Krstić, D. Živković, L. Balanović, T. Nonfer. Metal. Soc. **25** (8), 2630-2636 (2015).

[3] A. Urbańczyk-Gucwa, A. Brzezińska, K. Rodak, Arch. Metall. Mater. **63** (4), 2061-2066 (2018).

[4] K. Tian, B. Tian, A.A. Volinsky, Y. Zhang, Y. Liu, Y. Du, Arch. Metall. Mater. **63** (2), 875-882 (2018).

[5] W.A. Soffa, D.E. Laughlin, Prog. Mater. Sci. **49** (3-4), 347-366 (2004).

[6] E. Celik, A.K. Aslan, Arch. Metall. Mater. **63** (1), 299-305 (2018).

[7] V. Lebreton, D. Pachoutinski, Y. Bienvenu, Mater. Sci. Eng. A **508** (1-2), 83-92 (2009).

[8] J. Dutkiewicz, Met. Technol. **5** (1), 333-340 (1978).

[9] S. Nagarjuna, K. Balasubramanian, D.S. Sarma, Radiother. Oncol. **36** (8), 1058-1066 (1995).

[10] X.H. Wang, C.Y. Chen, T.T. Guo, J.T. Zou, X.Y. Yang, J. Mater. Eng. Perform. **24** (7), 2738-2743 (2015).

[11] J. Liu, X.H. Wang, Q.N. Ran, G. Zhao, X.X. Zhu, T. Nonfer. Metal. Soc. **26** (12), 3184-3188 (2016).

[12] R. Markandeya, S. Nagarjuna, D.S. Sarma, Mater. Sci. Eng. A **57** (4-5), 348-357 (2006).

[13] R. Markandeya, S. Nagarjuna, D.S. Sarma, J. Mater. Eng. Perform. **16** (5), 640-646 (2007).

[14] L. Chen, J.N. Han, B.W. Zhou, Y.Y. Xue, F. Jia, X.G. Zhang, T. Nonfer. Metal. Soc. **24** (4), 1046-1052 (2014).

[15] K. Maki, Y. Ito, H. Matsunaga, H. Mori, Scripta Mater. **68** (10), 777-780 (2013).

[16] G. Yang, Z. Li, Y. Yuan, Q. Lei, J. Alloy Compd. **640** (15), 347-354 (2015).

[17] R. Monzen, C. Watanabe, Mater. Sci. Eng. A **483-484** (15), 117-119 (2008).

[18] R. Markandeya, S. Nagarjuna, D.S. Sarma, Mater. Sci. Eng. A **371** (1-2), 291-305 (2004).

[19] R. Markandeya, S. Nagarjuna, D.V.V. Satyanarayana, D.S. Sarma, Mater. Sci. Eng. A **428** (1-2), 233-243 (2006).

[20] S. Semboshi, S. Sato, M. Ishikuro, K. Wagatsuma, A. Iwase, T. Takihiro, Metall. Mater. Trans. A **45** (8), 3401-3411 (2014).

[21] S. Nagarjuna, K. Balasubramanian, D.S. Sarma, J. Mater. Sci. **34** (12), 2929-2942 (1999).

[22] R. Markandeya, S. Nagarjuna, D.S. Sarma, J. Mater. Sci. **41** (4), 1165-1174 (2006).

[23] R. Markandeya, S. Nagarjuna, D.S. Sarma, Mater. Charact. **57** (4-5), 348-357 (2006).

[24] R. Markandeya, S. Nagarjuna, D.S. Sarma, Mater. Charact. **54** (4-5), 360-369 (2005).

[25] S. Semboshi, T. Al-kassab, R. Gemma, R. Kirchheim, Ultramicroscopy **109** (5), 593-598 (2009).

[26] F.L. Wang, Y.P. Li, K. Wakoh, Y. Koizumi, A. Chiba, Mater. Design **61**, 70-74 (2014).

[27] J. Liu, X.H. Wang, T.T. Guo, J.T. Zou, X.Y. Yang, Int. J. Min. Met. Mater. **22** (11), 1199-1204 (2015).

[28] M. Sobhani, A. Mirhabibi, H. Arabi, R.M.D. Brydson, Mater. Sci. Eng. A **577** (10), 16-22 (2013).

[29] I.S. Batra, A. Laik, G.B. Kale, G.K. Dey, U.D. Kulkarni, Mater. Sci. Eng. A **402** (1-2), 118-125 (2015).